[30]L. Berger and A. R. de Vroomen, J. Appl. Phys. 36, 2777 (1965).
[31]A. I. Schindler and B. C. La Roy, J. Appl. Phys. 37, 3610 (1966).
[32]S. Arajs, B. F. Oliver, and J. T. Michalak, J. Appl. Phys. 38, 1676 (1967).
[33]F. C. Schwerer and J. Silcox, Phys. Rev. B 1, 2391 (1970).
[34]F. C. Schwerer and L. J. Cuddy, Phys. Rev. B 2, 1575 (1970).
[35]R. C. Fivaz, J. Appl. Phys. 39, 1278 (1968).
[36]See, for example, Fig. 4 of J. Yahia and J. A. Marcus [Phys. Rev. 113, 137 (1959)] for gallium.
[37]A. K. Majumdar and L. Berger, J. Appl. Phys. 41, 1423 (1970).
[38]A. C. Ehrlich, R. Huguenin, and D. River, J. Phys. Chem. Solids 28, 253 (1967).
[39]H. Wagenblast and S. Arajs, Phys. Status Solidi 26, 409 (1968).
[40]H. Wagenblast and S. Arajs, J. Appl. Phys. 39, 5885 (1968).
[41]A. V. Gold, in *Proceedings of the International Conference on Magnetism, Nottingham*, 1964 (The Institute of Physics and the Physical Society, London, 1965), p. 124; J. Appl. Phys. 39, 768 (1968).
[42]N. E. Alekseevskii and Yu, P. Gaidukov, Zh. Eksp. Teor. Fiz. 41, 354 (1961) [Sov. Phys.-JETP 14, 256 (1962)].
[43]E. S. Borovik, Zh. Eksp. Teor. Fiz. 27, 355 (1954).
[44]M. T. Taylor, J. R. Merrill, and R. Bowers, Phys. Rev. 129, 2525 (1963).
[45]E. W. Collings and F. T. Hedgcock, Phys. Rev. 126, 1654 (1962).
[46]J. R. Anderson and A. V. Gold, Phys. Rev. 139, A1459 (1965).
[47]G. C. Carter and E. M. Pugh, Phys. Rev. 152, 498 (1966).

PHYSICAL REVIEW B VOLUME 7, NUMBER 9 1 MAY 1973

Spin-Orientation Diagrams and Magnetic Anisotropy of Rare-Earth–Iron Ternary Cubic Laves Compounds

U. Atzmony and M. P. Dariel
Nuclear Research Center, Negev, Beer Sheva, Israel

E. R. Bauminger, D. Lebenbaum, I. Nowik, and S. Ofer
The Racah Institute of Physics, The Hebrew University, Jerusalem, Israel

(Received 4 October 1972)

The directions of the easy magnetization in the $Ho_xTb_{1-x}Fe_2$, $Ho_xEr_{1-x}Fe_2$, $Dy_xTb_{1-x}Fe_2$, $Dy_xEr_{1-x}Fe_2$, and $Ho_xTm_{1-x}Fe_2$ systems have been determined, as a function of x and temperature by means of the Mössbauer effect in ^{57}Fe. If the direction of magnetization of each system is described by a (x,T) spin-orientation diagram, it is found that the (x,T) plane is divided into two or three regions, in each of which the direction of magnetization is along a different major crystal axis. Theoretical calculations based on the assumption that the magnetic crystalline anisotropy is due to the anisotropy of the interaction between the $4f$ electrons of the rare-earth ions with the crystal fields reproduced the general features of the experimental results though small discrepancies remained. Taking into account an additional contribution to the anisotropy attributed to the Fe-Fe interaction improved the agreement between the theoretical and experimental spin-orientation diagrams. From the theoretical fits to the experimental results a value of $(-0.038\pm0.003)a_0^{-2}$ is derived for the ratio of the crystal field parameters A_6/A_4. The transitions between the regions of the spin-orientation diagrams are not sharp. Possible reasons for the existence of the transition regions are discussed.

I. INTRODUCTION

Cubic Laves phases (type $MgCu_2$) are found in most rare-earth–iron binary systems. The magnetic properties of these compounds have been extensively investigated in recent years by neutron-diffraction, magnetic-susceptibility, and Mössbauer-effect measurements. All RFe_2 (R is a rare earth) compounds order magnetically and their magnetic ordering temperatures are around 600 K. Mössbauer studies on ^{57}Fe have shown that even though these compounds have an identical crystallographic structure, they present several types of spectra.[1] The appearance of the different spectra was accounted for in terms of the direction of the easy magnetization axis relative to the crystallographic axes of the unit cell in the respective compounds. With the direction of easy magnetization $\vec{n}$ along the [100] axis, all iron atoms are equivalent and a simple six-line spectrum is obtained, as was observed for $HoFe_2$ and $DyFe_2$. If $\vec{n}$ is along the [111] direction, two magnetically inequivalent iron sites with relative population 3 : 1 exist, giving rise to a spectrum which is a superposition of two six-line patterns, as observed for YFe_2, $TbFe_2$, $ErFe_2$, and $TmFe_2$. With $\vec{n}$ parallel

to the third major cubic axis, two magnetically inequivalent iron sites with a population ratio 2 : 2 are present, as observed in $SmFe_2$ at low temperatures.

Magnetic-anisotropy studies, usually carried out by torque measurements, require the use of carefully machined single-crystal specimens. Apart from the difficulties involved in growing single crystals of the reactive rare-earth intermetallic compounds, the extreme brittleness of these compounds renders any machining operation almost impossible. The Mössbauer effect offers, however, a simple experimental tool which allows a determination of the direction of the axes of easy magnetization in various compounds in polycrystalline form and the deduction of the magnetic-anisotropy parameters.

The magnetic anisotropy of rare-earth-containing alloys and compounds is ascribed mainly to the interaction of the crystal field with the $4f$ electrons of the rare-earth ions. In order to account for the occurrence of different preferred axes of magnetization in the various RFe_2 compounds, Bowden *et al.*[1] assumed that the magnetic anisotropy was due only to the rare-earth-ion anisotropy. Employing Bleaney's simple point-charge model and retaining only the fourth-order terms of the crystal field, Bowden *et al.* explained the observed directions of easy magnetization in almost all the binary RFe_2 compounds.

The initial objective of the present work was to gain further insight into the magnetic-anisotropy behavior of the rare-earth–iron compounds. This was done by the study of ternary systems of the type $R^1_xR^2_{1-x}Fe_2$ using the Mössbauer technique. The two binary Laves compounds R^1Fe_2 and R^2Fe_2 form a continuous pseudobinary solution. The measurements were carried out for systems in which R^1Fe_2 is magnetized in the [100] direction and R^2Fe_2 in the [111] direction. For each $R^1_xR^2_{1-x}Fe_2$ system the direction of easy magnetization as a function of x and temperature T has been determined. The results obtained for the direction of magnetization for each system have been described in terms of an (x, T) spin-orientation diagram.[2] The (x, T) plane is divided into two or three regions. In each of these regions the direction of magnetization is along one of the major crystal axes, [111], [110], or [100]. In the present work spin-orientation diagrams are presented for the $Ho_xTb_{1-x}Fe_2$, $Ho_xEr_{1-x}Fe_2$, $Dy_xTb_{1-x}Fe_2$, $Dy_xEr_{1-x}Fe_2$, and $Ho_xTm_{1-x}Fe_2$ systems. Comparison of the experimentally determined spin-orientation diagrams with the theoreticaly calculated ones permitted the determination of the ratio of the sixth- to fourth-order parameters of the crystal field at the rare-earth ions in the binary RFe_2 compounds. Some conclusions concerning the contribution of the anisotropy of the iron-iron interaction to the magnetic anisotropy of the RFe_2 compounds were also derived in the present work.

The results obtained for the $Ho_xTb_{1-x}Fe_2$ system and their theoretical analysis have already been published in letter form.[2]

II. EXPERIMENTAL PROCEDURES

The rare-earth metals used were supplied by Rare-Earth Products Ltd., England, and were stated to be 99.9% pure. The iron was of 99.99% nominal purity. The ternary compounds were prepared by arc melting in two stages under an argon atmosphere. First a homogeneous solid solution of the two rare-earth metals, with the desired composition ratio, was prepared. The alloy buttons were turned over and melted several times. In the second stage iron was added and the buttons were remelted twice. Weight losses were small and compensated for, assuming that they were due to the evaporation of the rare earths. Actually, the amounts of the rare earths were slightly larger than those required by the stoichiometric composition of the RFe_2 compounds, since this slight surplus prevented the formation of iron-containing intermetallic compounds other than the RFe_2 Laves phases. In most instances, the arc-melted buttons, wrapped in thin tantalum foils, were heat treated at 1100 °C for several days in evacuated quartz capsules. Powder diffraction patterns of each sample were obtained in a 114-mm Debye–Scherrer camera using iron filtered Co $K\alpha$ radiation. The determination of the lattice parameters enabled a rough check on the composition of the two rare-earth components to be made. A linear relationship (Vegard's law) was assumed to be valid in the pseudobinary solid solutions. Good agreement between nominal compositions and those deduced from lattice-parameter measurements was observed. About one-half of the samples (altogether 60 samples of different composition were prepared in the five ternary systems) were examined by metallographic and electron-microprobe analysis. The metallographic examination showed that all the samples contained less than 5% of foreign phases. The $L\alpha_1$ lines of the rare-earth components were used in microprobe analysis to check the composition and the homogeneity of the samples. True compositions were determined by applying standard correction procedures to the electron-microprobe data.[3] The homogeneity with respect to the distribution of the rare-earth components was found to be better than 2% in all samples.

The spectra were obtained using a constant-acceleration-type spectrometer. The temperature of the absorber was stabilized within 1 K. The source used was ^{57}Co in palladium at room temperature.

III. RESULTS

Mössbauer-effect measurements of the 14.4-keV γ-ray transition of ^{57}Fe were carried out in a series of absorbers belonging to the ternary systems $R^1_x R^2_{1-x}Fe_2$ (R^1 = Dy, R^2 = Tb, Er, and Tm) at various temperatures between 4.2 and 300 K. Some examples of the experimental spectra are shown in Figs. 1–3. Spectra of the $Ho_xTb_{1-x}Fe_2$ system were shown in Figs. 2 and 3 of Ref. 2. In Fig. 1 the three main types of spectra obtained are shown. Spectra of type *a* are characterized by a simple six-line pattern while those of types *b* and *c* are a superposition of two six-line patterns with relative intensities 1 : 3 and 2 : 2, respectively. Spectra of the same type correspond to compounds in which $\vec{n}$ has the same direction with respect to the crystallographic axes. Most of the experimental spectra are of one of the three types described above.

The rare-earth ions in the RFe_2 compounds are situated on a diamond sublattice and have a cubic site symmetry. The iron ions, lying on a corner sharing network of regular tetrahedra, have a $\bar{3}m$ site symmetry, with the threefold axes parallel to the ⟨111⟩ directions. The ligand-electric-field-gradient (EFG) tensor at the iron nuclei is axially symmetric. The axes of the gradients are parallel to the local threefold axes of symmetry.

Spectra of type *a* are obtained when $\vec{n}$, the direction of magnetization, is parallel to the [100] direction and thus forms an angle of 54°44′ with all four ⟨111⟩ directions. All iron ions are equivalent and yield the simple six-line pattern.

When $\vec{n}$ is parallel to a [111] direction, it forms an angle $\theta = 0°$ with the axis of the EFG acting on one iron nucleus of each tetrahedron and an angle of $\theta = 70°32'$ with the axes of the EFG's of the three other iron nuclei of this tetrahedron. There are

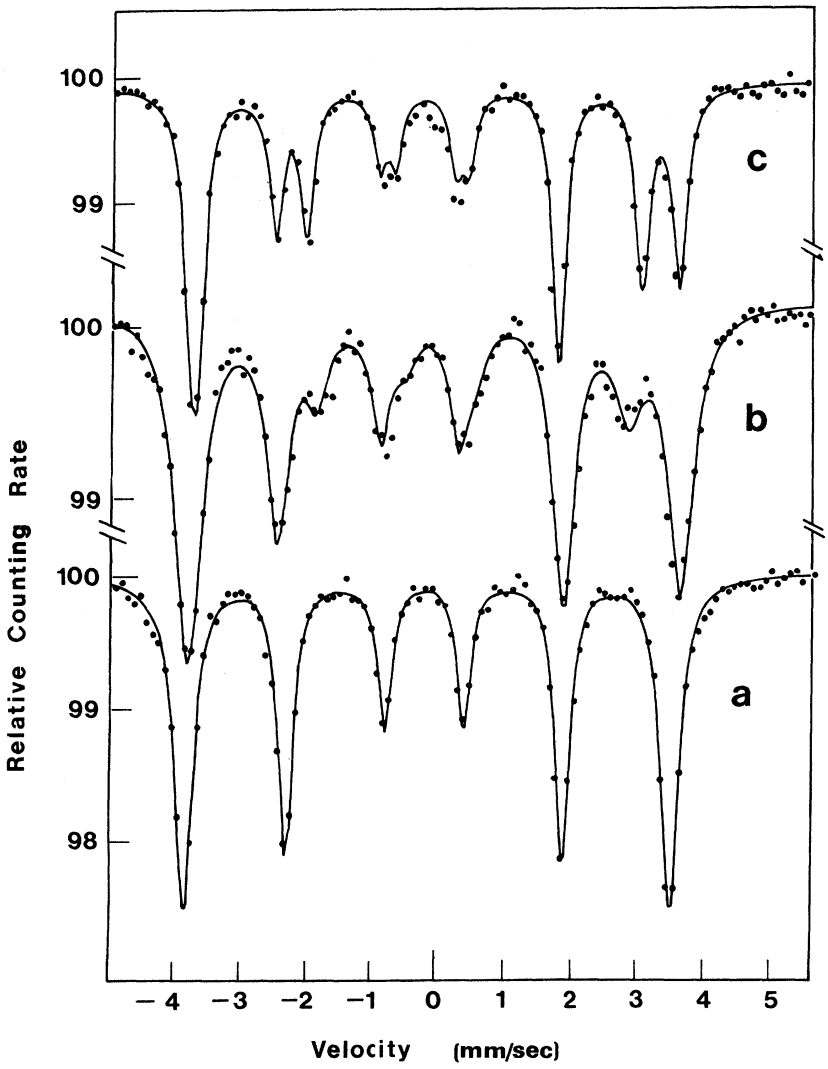

FIG. 1. Three typical Mössbauer spectra. Spectrum *a* is a simple six-line spectrum characteristic of the [100] direction of magnetization (spectrum of $Ho_{0.8}Er_{0.2}Fe_2$). Spectrum *b* is a superposition of two six-line spectra with intensity ratio 3 : 1, characteristic of the [111] direction of magnetization (spectrum of $Ho_{0.3}Er_{0.7}Fe_2$ at 4.2 K). Spectrum *c* is a superposition of two six-line spectra of equal intensity characteristic of the [110] direction of magnetization (spectrum of $Ho_{0.75}Er_{0.25}Fe_2$ at 4.2 K).

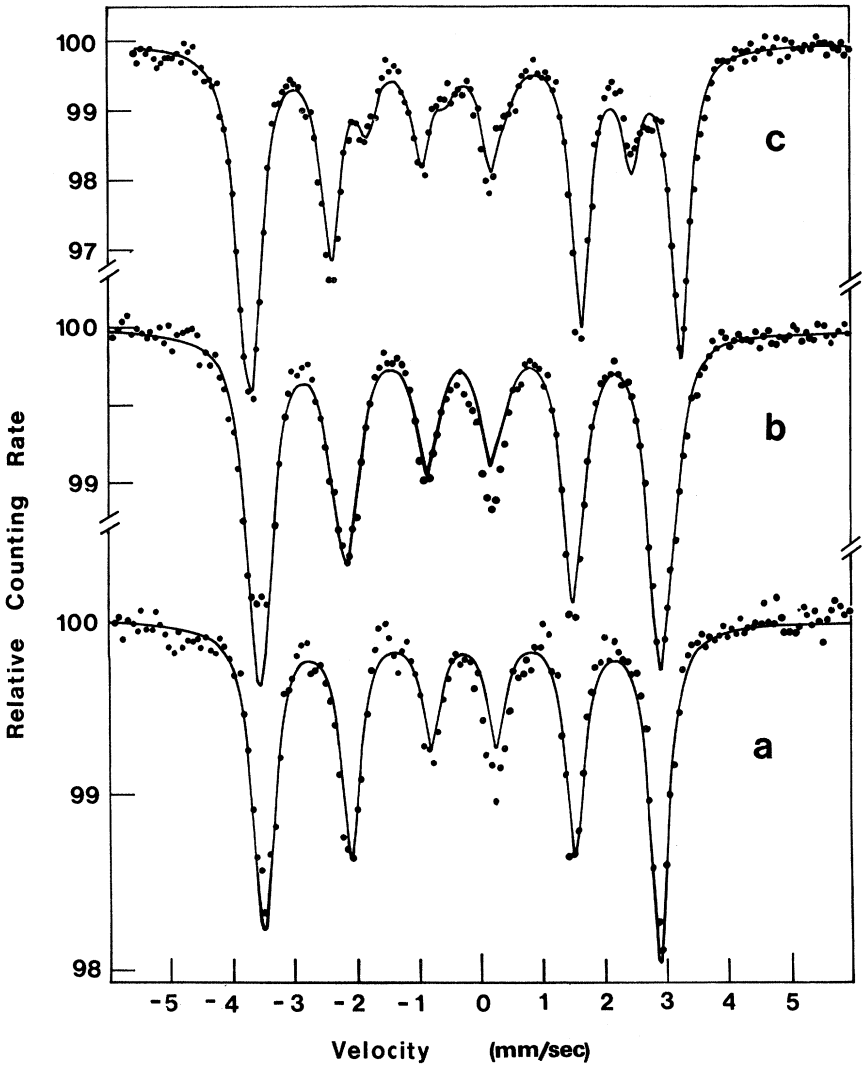

FIG. 2. Mössbauer spectra of $Dy_xEr_{1-x}Fe_2$ at 300 K. (a) corresponds to $x=0.2$, (b) to $x=0.15$, and (c) to $x=0.1$.

thus two inequivalent iron sites with population ratio 1 : 3 giving rise to spectra of type b.

When $\vec{n}$ is in the [110] direction, it forms an angle $\theta=35°15'$ with the axes of the EFG acting on two iron nuclei of each tetrahedron and an angle $\theta=90°$ with the axes of the EFG at the other two iron nuclei. There are again two inequivalent iron sites with population ratio 2 : 2 giving spectra of type c. If the magnetization is in an arbitrary direction, the four iron sites will usually be inequivalent and spectra different from the abovementioned three types will be obtained. The following two factors are the reason for the dependence of the hyperfine interaction of a Fe nucleus on the angle θ between $\vec{n}$ and the axis of local symmetry at its site: (i) The contribution of the quadrupole interaction to the hyperfine splittings depends on θ; (ii) the contribution of the dipolar magnetic fields to the magnetic hyperfine field at the Fe nucleus also depends on θ.

As can be observed in Fig. 1, the difference between the three types of Mössbauer spectra (due to sufficiently different hyperfine splittings at inequivalent iron sites) allows the determination of the direction of easy magnetization of the great majority of the samples by simple visual inspection. Nevertheless, computer least-squares-fit analysis was applied to most experimental Mössbauer spectra. Good agreement was achieved between the experimental spectra and theoretical ones based on a Hamiltonian of the complete hyperfine interaction, proving the validity of the model employed. In this analysis linewidths, isomer shifts, and quadrupole interactions were assumed to have the same value at inequivalent iron sites. The least-squares-fit analysis yielded nearly constant values for these quantities in all the examined spectra.

The experimental results for the various pseudobinary systems investigated in the present study are summarized in (x, T) spin-orientation dia-

grams. In these diagrams, the (x, T) plane is divided into two or three regions. In each of these regions, the direction of magnetization is along one of the major crystal axes, [111], [100], or [110]. The transitions between the regions are not sharp. Spectra belonging to these transition regions cannot be ascribed to one of the three types shown in Fig. 1. In Fig. 2, a series of Mössbauer spectra of the $Dy_xEr_{1-x}Fe_2$ system at room temperature is shown. The change of the direction of magnetization from the [100] to the [111] direction can be seen to take place for $0.1 < x < 0.2$. Figure 2(b) is an example of an intermediate type of spectra characteristic of the transition region. In Fig. 3 a series of spectra of $Ho_{0.6}Tm_{0.4}Fe_2$ at different temperatures is shown. The change of direction of magnetization can clearly be seen to take place at $T = 56 \pm 5$ K.

The spin-orientation diagrams of the $Ho_xTb_{1-x}Fe_2$, $Ho_xEr_{1-x}Fe_2$, and $Ho_xTm_{1-x}Fe_2$ systems are shown in Figs. 4–6. In these three pseudobinary systems there exists, at low temperature and intermediate

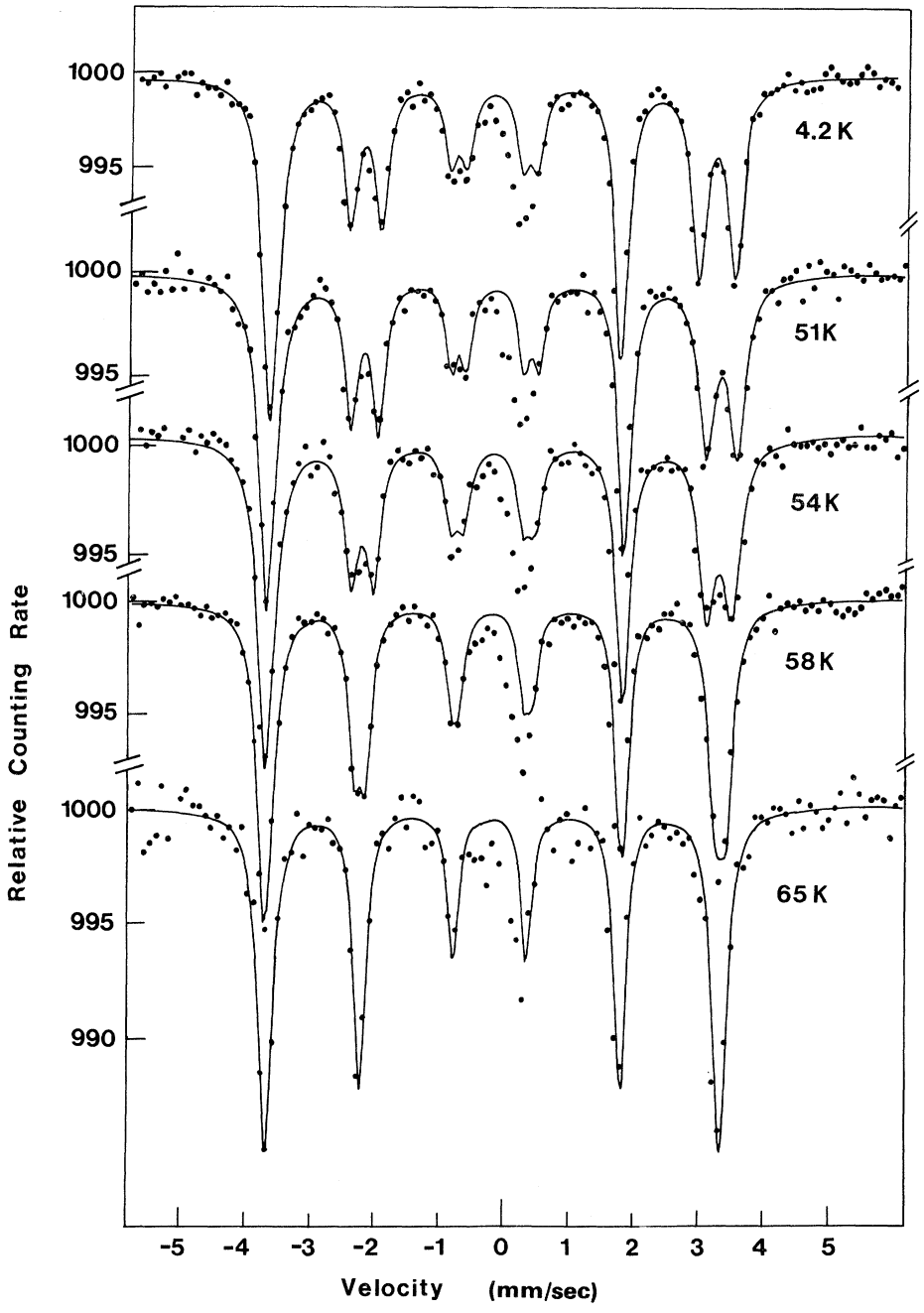

FIG. 3. Mössbauer spectra of $Ho_{0.6}Tm_{0.4}Fe_2$ at various temperatures.

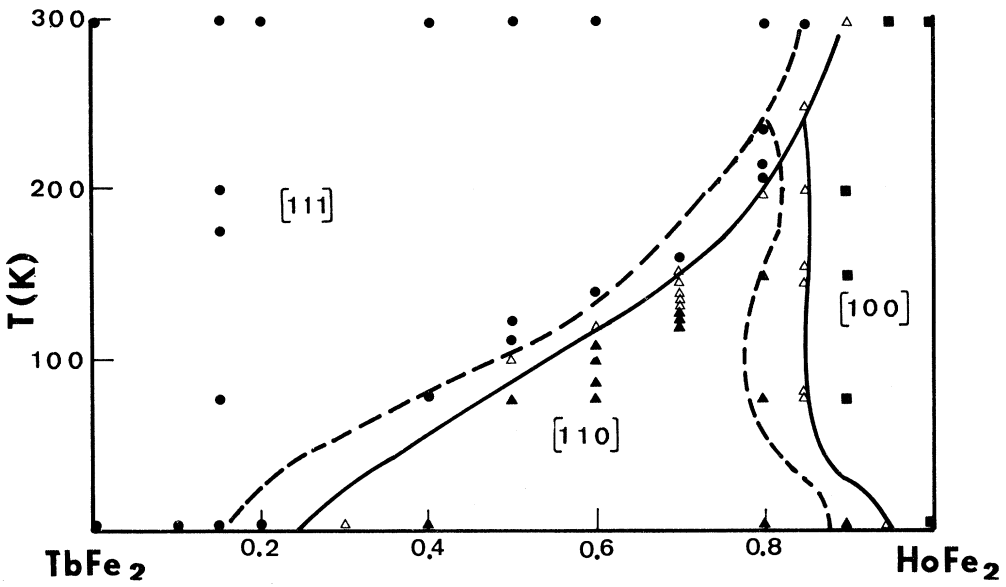

FIG. 4. Spin-orientation diagram of the $Ho_xTb_{1-x}Fe_2$ system. Filled circles, filled triangles, and filled squares correspond to experimentally determined spectra characteristic of the [111], [110], and [100] axes of magnetization, respectively. Open triangles correspond to intermediate types of spectra. The solid lines are experimentally determined boundaries of regions with different directions of magnetization. The dashed lines are the boundaries determined theoretically using the one-ion model (copied from Ref. 2).

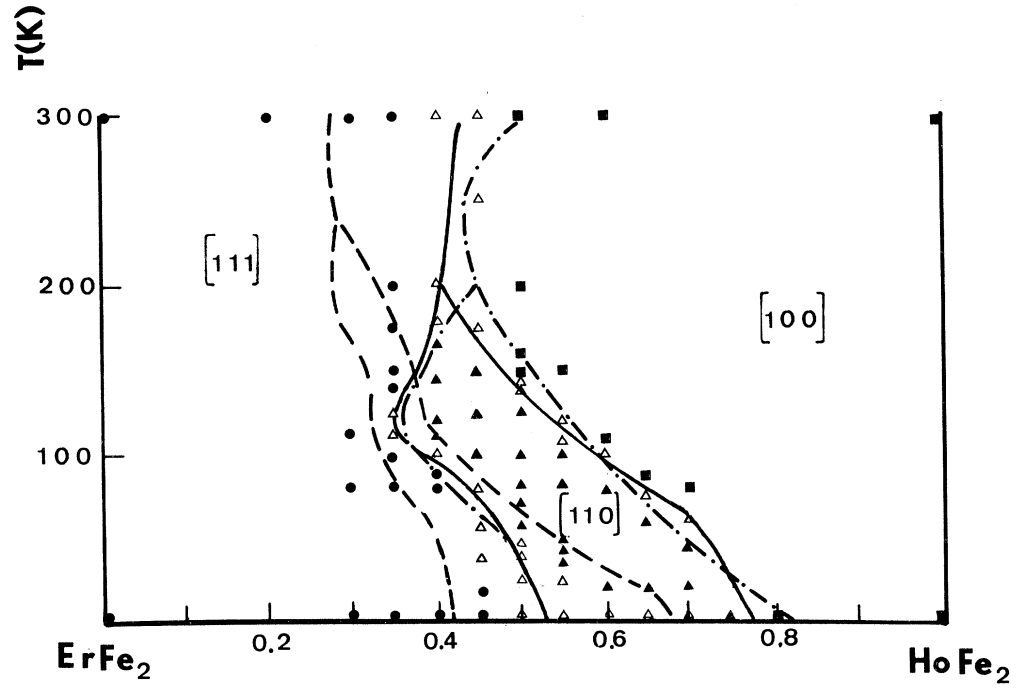

FIG. 5. Spin-orientation diagram of the $Ho_xEr_{1-x}Fe_2$ system. Filled circles, filled triangles, and filled squares correspond to experimentally determined spectra characteristic of the [111], [110], and [100] axes of magnetization, respectively. Open triangles correspond to intermediate types of spectra. The solid lines are experimentally determined boundaries of regions with different directions of magnetization. The dashed lines are the boundaries determined theoretically using the one-ion model. The dot-dashed curves are the theoretical boundaries, corrected for a rare-earth independent (Fe-Fe) anisotropic interaction deduced from the $Ho_xTb_{1-x}Fe_2$ diagram.

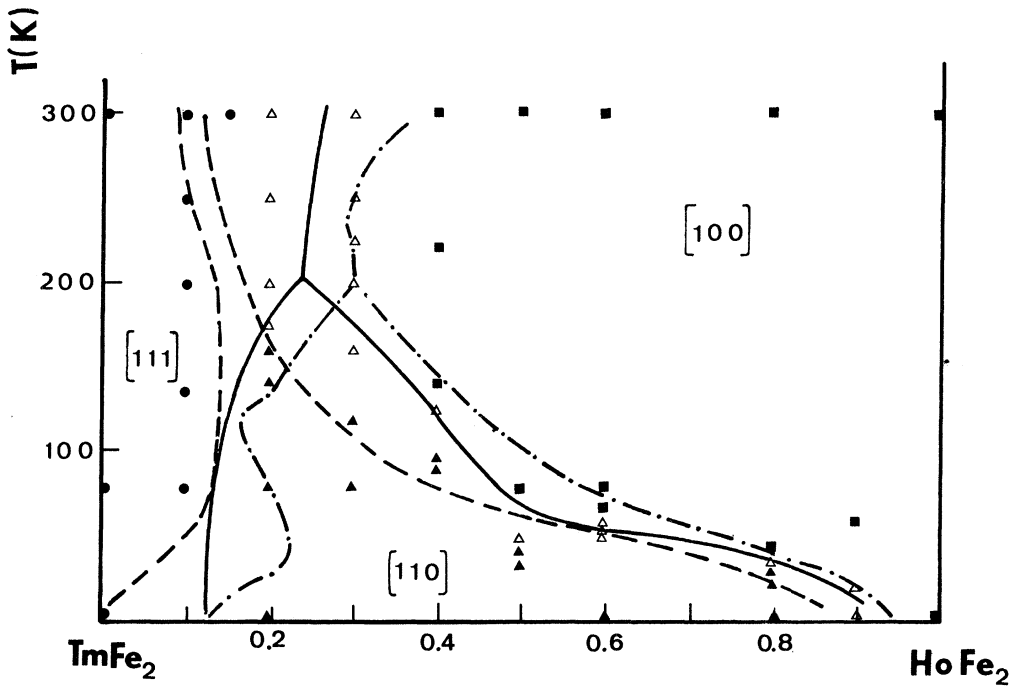

FIG. 6. Spin-orientation diagram of the $Ho_xTm_{1-x}Fe_2$ system.

compositions, a region with $\vec{n}$ in the [110] direction, even though in the binary compound $HoFe_2$, $\vec{n}$ is in the [100] direction, and in $TbFe_2$, $ErFe_2$, and $TmFe_2$ $\vec{n}$ is in the [111] direction throughout the whole temperature range. The spin-orientation diagrams of the $Dy_xTb_{1-x}Fe_2$ and $Dy_xEr_{1-x}Fe_2$ systems are shown in Figs. 7 and 8. In these two systems, the (x, T) plane is divided into two regions only, and there is no region in which $\vec{n}$ is in the [110] direction.

IV. DISCUSSION

Theoretical Spin-Orientation Diagrams: One-Ion Model

Rare-earth-containing alloys or compounds usually exhibit extremely high magnetocrystalline

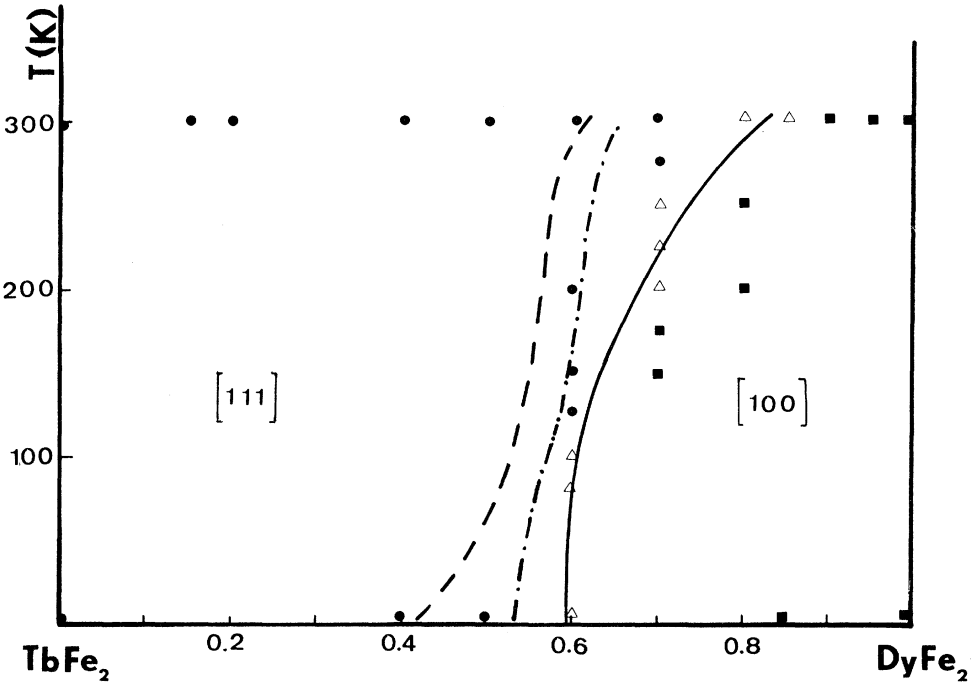

FIG. 7. Spin-orientation diagram of the $Dy_xTb_{1-x}Fe_2$ system.

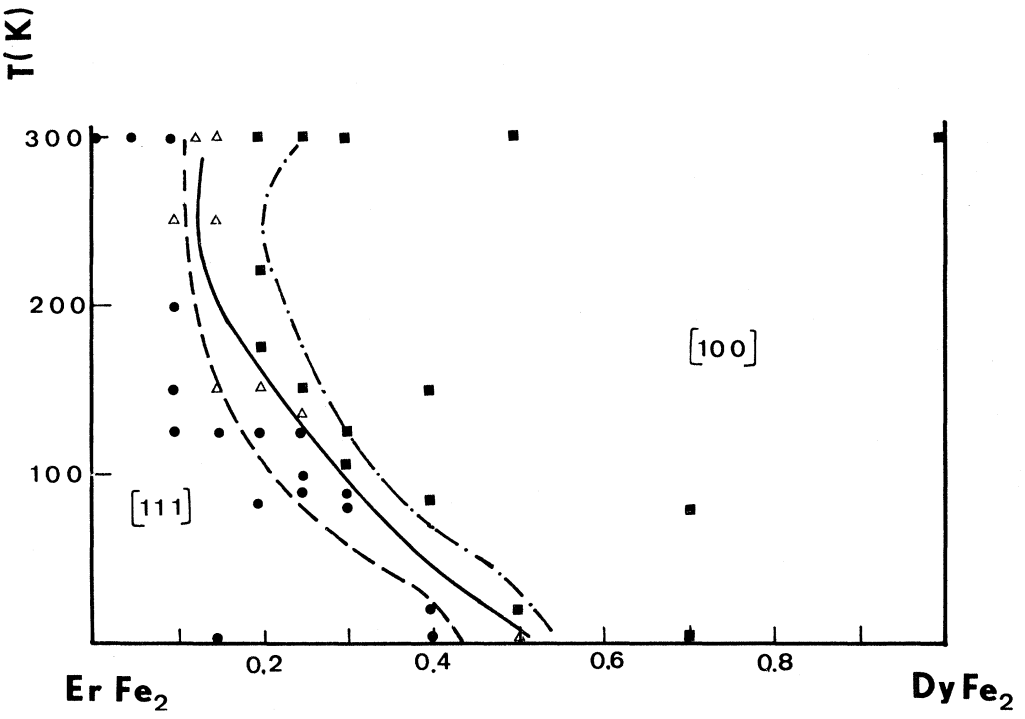

FIG. 8. Spin-orientation diagram of the $Dy_xEr_{1-x}Fe_2$ system.

anisotropies. These are attributed mainly to the anisotropy of the interaction between the well-shielded $4f$ electrons of the rare-earth ions with the crystal field.

The Hamiltonian of a single rare-earth ion in a crystal can be written as

$$\mathcal{H} = \mathcal{H}_0 + \mathcal{H}_{\text{exch}} + \mathcal{H}_{\text{crys}} , \tag{1}$$

where $\mathcal{H}_0$ includes the electrostatic and the spin-orbit interaction, $\mathcal{H}_{\text{exch}}$ is the Hamiltonian of the exchange interaction, and $\mathcal{H}_{\text{crys}}$ represents the interaction of the crystalline electric field produced by the surrounding ions with the $4f$ electrons in the partially filled shell. $\mathcal{H}_0$ is isotropic, whereas the anisotropic part of the Hamiltonian is $\mathcal{H}_{\text{exch}} + \mathcal{H}_{\text{crys}}$. Neglecting the R-R interaction, the total anisotropic part of the Hamiltonian per unit volume is

$$\mathcal{H}_{\text{anis}} = \sum_R (\mathcal{H}_{\text{exch}} + \mathcal{H}_{\text{crys}}) = N(\mathcal{H}_{\text{exch}} + \mathcal{H}_{\text{crys}}) , \tag{2}$$

where N is the number of rare-earth ions per unit volume.

For most rare-earth ions $\mathcal{H}_{L\text{-}S} \gg \mathcal{H}_{\text{crys}}$, $\mathcal{H}_{\text{exch}}$ and J is a good quantum number. (This assumption is not valid for Sm^{3+} and Eu^{2+} ions, whose first excited state lies relatively close above the ground state). Within a single J manifold $\mathcal{H}_{\text{exch}}$ can be expressed as

$$\mathcal{H}_{\text{exch}} = 2(g_J - 1)\mu_B H_{\text{exch}}(T)\vec{\mathbf{J}} \cdot \vec{\mathbf{n}} , \tag{3}$$

where $H_{\text{exch}}(T)$ is the exchange field acting on the rare-earth ion. In expressing $\mathcal{H}_{\text{exch}}$ in the above form it is assumed that the exchange interaction itself is isotropic. (In the general case $H_{\text{exch}} = k\vec{\vec{\lambda}} \cdot \vec{\mathbf{n}}$, where $\vec{\vec{\lambda}}$ is the anisotropy exchange tensor. For an isotropic exchange interaction $\vec{\vec{\lambda}}$ is a unit tensor.)

The Hamiltonian of the cubic crystal field interaction can be written as

$$\mathcal{H}_{\text{crys}} = V_4 + V_6 , \tag{4}$$

where

$$V_4 = A_4(1 - \sigma_4)\langle r^4 \rangle \langle J || \beta || J \rangle (O_4^0 + 5O_4^4)$$

and

$$V_6 = A_6 \langle r^6 \rangle \langle J || \gamma || J \rangle (O_6^0 - 21O_6^4) ,$$

where O_n^m are the operator equivalents, and β and γ the reduced matrix elements tabulated by Hutchings.[4] The values of $\langle r^n \rangle$ used were those calculated for the different rare-earth ions by Freeman and Watson.[5] A_4 and A_6, the crystal field parameters, are assumed to be independent of the rare-earth ions involved, which are all trivalent. The value of the shielding parameters σ_4 used were those calculated for the various rare-earth ions by Freeman and Watson.[6]

In calculating the theoretical spin-orientation diagrams using Eqs. (2)–(4), it was assumed that the R-R interactions are small compared to the R-Fe interactions and can be neglected. This assumption is supported by results of Mössbauer-effect measurements on ^{169}Tm in $TmFe_2$[7] and ^{161}Dy in

$DyFe_2$.[8] The temperature dependences of the hyperfine fields acting on the rare-earth nuclei in these compounds can be fitted by Brillouin functions with J of the respective rare-earth ion and exchange fields proportional to the hyperfine fields acting on the iron nuclei at the various temperatures. Furthermore, the ordering temperatures of all RFe_2 compounds are much higher than the respective ordering temperatures of the isostructural RCo_2 and RNi_2 compounds, indicating that the R-R interactions are much smaller than the Fe-Fe and R-Fe interactions. This leads to the conclusion that in first approximation H_{exch} at the rare-earth ion is independent of the rare-earth ion involved and has the same temperature dependence as H_{eff} acting on the iron nuclei. This temperature dependence can be approximated by the expression

$$H_{exch}(T) = H_{exch}(0)(1 - 0.1T/300) \tag{5}$$

for temperatures between 0 and 300 K.

This expression is derived from the temperature dependence of the hyperfine field acting on ^{57}Fe nuclei in $DyFe_2$ as determined by Mössbauer-effect measurements,[8] and of the iron sublattice magnetization in $ErFe_2$ as determined by neutron diffraction.[9] The eigenvalues ϵ_i of the Hamiltonian [Eqs. (2)–(4)] of the binary compounds RFe_2 were calculated for the three possible directions $(\vec{n}_j)$ of the easy magnetization ([111], [110], and [100]) and for various values of the parameters A_4, A_6, and $H_{exch}(0)$. As mentioned above, these parameters are assumed to have the same values for all the binary Laves compounds of the rare earths investigated. The magnetocrystalline free energy per unit volume $F_R(\vec{n}_j, T)$ of the binary compound RFe_2 is given by

$$F_R(\vec{n}_j, T) = -kTN\ln Z, \tag{6}$$

where $Z(T, \vec{n}_j)$ is the partition function

$$Z(T, \vec{n}_j) = \sum_{i=1}^{J} e^{-\epsilon_i/kT}. \tag{7}$$

For the ternary $R_x^1 R_{1-x}^2 Fe_2$ compounds, the magnetocrystalline free energy can be expressed by

$$F(x, \vec{n}_j, T) = xF_{R^1}(\vec{n}_j, T) + (1-x)F_{R^2}(\vec{n}_j, T). \tag{8}$$

The easy direction of magnetization of a given compound at a given temperature is the direction $(\vec{n}_j)$ for which the expression (8) has the lowest value. This procedure was repeated for various values of x and T and used to construct spin-orientation diagrams. These diagrams depend on the values chosen for the three parameters A_4, A_6, and $\mu_B H_{exch}(0)$.

Comparison with the experimental spin-orientation diagrams (Figs. 4–8) indicates that A_6 cannot be neglected and that the ratio $A_6/A_4 = -(0.038 \pm 0.003)a_0^{-2}$ fits the experimental data best (if $A_6 = 0$, the theoretical spin-orientation diagrams do not include a region with $\vec{n}$ in the [100] direction). The theoretical spin-orientation diagrams of the Ho compounds are sensitive to the ratio of A_6/A_4 (as shown, for instance, in Fig. 9), but not to the exact values of A_4 and $\mu_B H_{exch}$. The experimental results could be fitted with values of A_4 between 10 and 50 K/a_0^4. The value of $\mu_B H_{exch}(0)$ was chosen as -150 K. This value is derived from previous Mössbauer-effect measurements carried out on RFe_2 compounds.[8,10] The theoretical spin-orientation diagrams were not sensitive to the exact value of $\mu_B H_{exch}(0)$ in the range between -100 and -160 K. (The spin orientation diagrams of the Dy-containing compounds are much less sensitive to the value of A_6/A_4 than those of the Ho-containing compounds.) The theoretical spin-orientation diagrams with $A_4 = 10$ K/a_0^4, $A_6/A_4 = -0.04a_0^{-2}$, and $\mu_B H_{exch}(0) = -150$ K are shown in Figs. 4–8 (dashed lines).

Bulk Magnetic Anisotropy Constants

The magnetic anisotropy properties of crystals are often expressed in terms of the bulk magnetic anisotropy constants. The bulk magnetocrystalline free energy in cubic structures can be expanded in a polynomial series in α_i, the direction cosines of the direction of magnetization with respect to the cube edges:

$$F_R = K_0 + K_1(\alpha_1^2\alpha_2^2 + \alpha_2^2\alpha_3^2 + \alpha_3^2\alpha_1^2) + K_2(\alpha_1^2\alpha_2^2\alpha_3^2) + \cdots, \tag{9}$$

where K_0, K_1, and K_2 are the bulk anisotropy constants. The easy direction of magnetization is the one that minimizes F_R. F_R has extremum values for the directions parallel to the major axes of symmetry of the cubic system, namely, the [100], [110], and [111] directions. Whether these extrema are minima or maxima, depends on the values of K_1 and K_2. The values of K_1 and K_2 can be deduced from the values of the magnetocrystalline free energy of the binary Laves compounds RFe_2 for the three possible directions of the easy magnetization, using the following relationships:

$$K_1(T) = [4F_R(\vec{n}_2, T) - 4F_R(\vec{n}_1, T)], \tag{10}$$

$$K_2(T) = [27F_R(\vec{n}_3, T) - 36F_R(\vec{n}_2, T) + 9F_R(\vec{n}_1, T)], \tag{11}$$

where $\vec{n}_1$, $\vec{n}_2$, and $\vec{n}_3$ are unit vectors parallel to the [100], [110], and [111] directions, respectively.

The values of $F_R(\vec{n}_j, T)$ strongly depend on the exact values of the parameters A_4, A_6/A_4, and $\mu_B H_{exch}(0)$. As previously mentioned, only A_6/A_4 could be accurately determined from our measurements, whereas the parameters A_4 and $\mu_B H_{exch}(0)$ could not be determined accurately. Values of K_1 and K_2 for the various binary RFe_2 compounds, calculated on the basis of the one-ion model, using

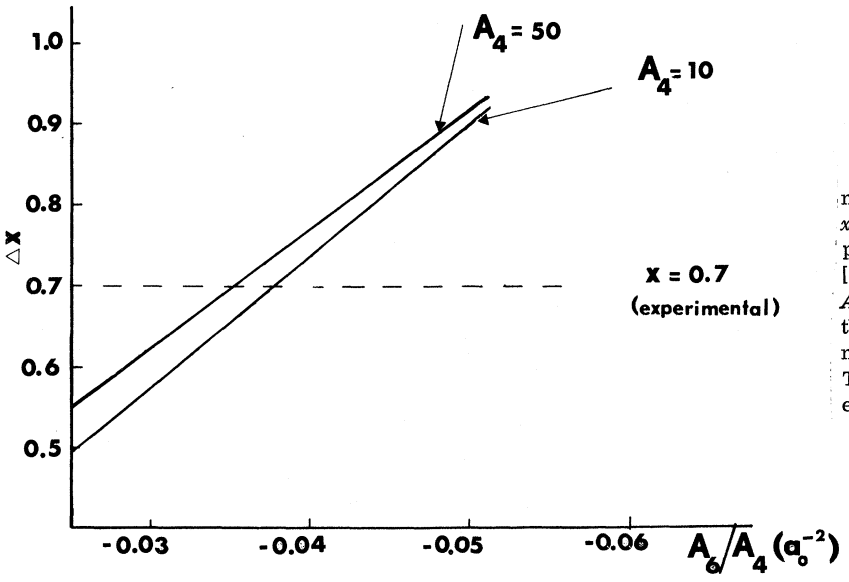

FIG. 9. Difference (Δx) between maximum and minimum values of x for which the $Ho_x Tb_{1-x}Fe_2$ compounds are magnetized at 4.2 K, in the [110] direction, as a function of A_6/A_4. Solid lines represent the theoretical values of Δx (one-ion model) for various of A_4 (in K/a_0^4 units). The dashed line represents the experimental value of Δx.

the value $-0.04a_0^{-2}$ for A_6/A_4, the value 150 K for $\mu_B H_{exch}$, and the value of 10 K/a_0^4 for A_4, are given in Table I for 4.2, 80, and 300 K. Values of the bulk anisotropy constants of similar orders of magnitude have been found in rare-earth garnets[11] and other rare-earth compounds exhibiting high magnetocrystalline anisotropy.

Additional Contributions to the Magnetic Anisotropy

Though the theory, just outlined, reproduces the main feature of the experimental spin-orientation diagrams, several systematic deviations are still observed. The experimental extension of the [111] regions seems in all instances to be larger than that predicted by the one-ion model. This feature is particularly salient in the $Ho_xTb_{1-x}Fe_2$ system, in which the theoretical boundaries of the various regions are laterally shifted with respect to the experimentally determined boundaries, supposed to lie in the middle of the transition regions.

The shift between the experimental and theoretical boundaries in the spin-orientation diagrams may be due to several factors. The main factor is probably the neglect in the theoretical calculations of an anisotropy term, contributed by the Fe-Fe interaction, which favors the [111] direction (as demonstrated by the fact that in YFe_2[1] and $ZrFe_2$[12] the easy magnetization is in the [111] direction). Disagreements between the theoretical and experimental spin-orientation diagrams may also be caused by the uncertainty in the values of some of the parameters ($\langle r^n \rangle$, antishielding factors) used in the calculations, and by the anisotropy of the exchange interactions. Finally, the disagreement may be due to the neglect of other noncubic anisotropy terms, such as dipolar fields or distortions, that were not taken into account in Eq. (1). The effect of distortions in particular may be nonnegligible, as shown recently by the giant magnetostrictive effects observed in binary RFe_2 compounds.[13] Efforts have been made to check whether mixing of the higher ionic J levels into the ground level has any effect on the shape of the theoretical spin-orientation diagrams. Calculations taking into account such mixing were carried out and have shown that this mixing has an absolutely negligible effect on the theoretical diagrams.

In order to improve the fit between the theoretical and experimental spin-orientation diagrams, it was assumed that the disagreement between them is produced only by the anisotropy of the Fe-Fe interaction, which would be the same for all RFe_2 compounds. The additional free energies in the [100], [110], and [111] directions at various temperatures which are needed in order to get a perfect overlap between the theoretical and experimental spin-orientation diagrams in the $Ho_xTb_{1-x}Fe_2$ system have been calculated. The values of these additional free energies $F_{add}(\vec{n}_j, T)$ obtained for this system

TABLE I. Values of the bulk anisotropy constants K_1 and K_2 for the various binary RFe_2 compounds at 4.2, 80, and 300 K, calculated on the basis of the one-ion model using the values $-0.04a_0^{-2}$ for A_0/A_4, -150 K for $\mu_B H_{exch}(0)$, and 10 K/a_0^4 for A_4.

	K_1 (10^6 erg/cm^3)			K_2 (10^6 erg/cm^3)		
Compound	4.2 K	80 K	300 K	4.2 K	80 K	300 K
$HoFe_2$	20	33	2	1173	201	0.78
$DyFe_2$	251	133	7.2	−606	−187	−1.5
$ErFe_2$	−39	−29	−0.77	−896	−86	−0.16
$TbFe_2$	−170	−118	−11	157	77	1.1
$TmFe_2$	−193	−22	−0.25	454	12	0.01

were then used to obtain corrected spin-orientation diagrams in all other systems. [Actually, only the differences, $F_{add}(\vec{n}_2, T) - F_{add}(\vec{n}_1, T)$ and $F_{add}(\vec{n}_3, T) - F_{add}(\vec{n}_1, T)$ can be determined by the fitting of the theoretical to the experimental spin-orientation diagrams of the $Ho_xTb_{1-x}Fe_2$ system and only these differences are relevant in calculating theoretical spin-orientation diagrams.]

The following relation between the free energies at a point (x_1, T) lying on the boundary between the [111] and the [100] regions in the spin-orientation diagram of the $Ho_xTb_{1-x}Fe_2$ system must hold to give a perfect fit between the experimental and theoretical spin-orientation diagrams:

$$x_1 F_{Ho}(\vec{n}_3, T) + (1-x_1)F_{Tb}(\vec{n}_3, T) + F_{add}(\vec{n}_3, T) = x_1 F_{Ho}(\vec{n}_2, T) + (1-x_1)F_{Tb}(\vec{n}_2, T) + F_{add}(\vec{n}_2, T). \quad (12)$$

Similarly for a transition point (x_2, T) between the [110] and the [100] regions, the relation

$$x_2 F_{Ho}(\vec{n}_2, T) + (1-x_2) F_{Tb}(\vec{n}_2, T) + F_{add}(\vec{n}_2, T) = x_2 F_{Ho}(\vec{n}_1, T) + (1-x_2) F_{Tb}(\vec{n}_1, T) + F_{add}(\vec{n}_1, T) \quad (13)$$

must hold, and finally for a transition point (x_3, T) between the [111] and [100] region, the relation

$$x_3 F_{Ho}(\vec{n}_3, T) + (1-x_3) F_{Tb}(\vec{n}_3, T) + F_{add}(\vec{n}_3, T) = x_3 F_{Ho}(\vec{n}_1, T) + (1-x_3)F_{Tb}(\vec{n}_1, T) + F_{add}(\vec{n}_1, T) \quad (14)$$

must hold.

By solving Eqs. (12) and (13) the values of $F'_{add}(\vec{n}_2, T) = F_{add}(\vec{n}_2, T) - F_{add}(\vec{n}_1, T)$ and $F'_{add}(\vec{n}_3, T) = F_{add}(\vec{n}_3, T) - F_{add}(\vec{n}_1, T)$ were determined as a function of T for temperatures between 4 K and the temperature corresponding to the triple point in the spin-orientation diagram. Using Eq. (14) the values of $F'_{add}(\vec{n}_3, T)$ were determined for temperatures between the temperature corresponding to the triple point and 300 K. The values used for $F_{Ho}(\vec{n}_j, T)$ and $F_{Tb}(\vec{n}_j, T)$ were those determined previously, on basis of the one-ion model, assuming $A_4 = 10$ K$/a_0^4$, $A_6/A_4 = -0.040 a_0^{-2}$, and $\mu_B H_{exch}(0) = -150$ K.

From the values derived for $F'_{add}(\vec{n}_2, T)$ and $F'_{add}(\vec{n}_3, T)$, values of the additional bulk anisotropy constants $K_1^{add}(T)$ and $K_2^{add}(T)$ can be calculated using Eqs. (10) and (11). The values of $K_1^{add}(T)$ and $K_2^{add}(T)$ as calculated from the $Ho_xTb_{1-x}Fe_2$ system for 4.2, 80, and 220 K are given in Table II.

Assuming the additional anisotropy energy to be independent of the rare-earth ions involved, the values of $F'_{add}(\vec{n}_2, T)$ and $F'_{add}(\vec{n}_3, T)$ found for the $Ho_{1-x}Tb_xFe_2$ system were used in all other ternary systems to obtain corrected spin-orientation diagrams. The agreement between the experimental spin-orientation diagrams and the theoretical diagrams is improved in all cases, showing that the anisotropy of the Fe-Fe exchange interaction (independent of R) should indeed not be neglected. Very good agreement is obtained in the $Ho_xEr_{1-x}Fe_2$ system (Fig. 5). In the $Ho_xTm_{1-x}Fe_2$ (Fig. 6) and the $Dy_xTb_{1-x}Fe_2$ (Fig. 7) systems, the agreement between theory and experimental data is improved though it is not perfect. In the $Dy_xEr_{1-x}Fe_2$ (Fig. 8) system the corrected theoretical boundary line is to the right of the experimental boundary line, whereas the noncorrected theoretical curve lies to the left of the experimental line.

Attempts were made to improve the fit between the experimental and theoretical spin-orientation diagrams by following the above procedure for determining $F'_{add}(\vec{n}_j, T)$ and using values of A_4, A_6/A_4, and $\mu_B H_{exch}(0)$ different from those mentioned above. Theoretical spin-orientation diagrams were calculated for values of $10 \leq A_4 \leq 50$ K$/a_0^4$ and $-160 \leq \mu_B H_{exch}(0) \leq -110$ K and various values of A_6/A_4. The theoretical diagrams [including $F'_{add}(\vec{n}_j, T)$ corrections] were found to be insensitive to the values of A_4 and $\mu_B H_{exch}(0)$. The best agreement was again obtained for $A_6/A_4 = -0.038 \pm 0.003 a_0^{-2}$.

On the basis of susceptibility studies on single crystals of cubic Laves $ErAl_2$ samples, Purwins[14] deduced a value of $A_6/A_4 = -0.008 a_0^{-2}$. Values of A_6/A_4 and of A_4 deduced from a point-charge calculation similar to that of Bleaney[15] are shown in Table III for various possible charge states of the iron ions. It appears that the point-charge model is in reasonable agreement with the experimentally determined values of A_6/A_4 for a charge state of the iron ion between +1 and +2. The value of A_4 for this charge state is within the range taken in this study for the theoretical spin-orientation determination. No results concerning the crystal field parameters of rare-earth iron Laves compounds are available.

The persisting disagreement between the theoretical and experimental spin-orientation diagrams for some of the systems indicate that $F'_{add}(\vec{n}_j, T)$ is not entirely due to the Fe-Fe interaction, but depends also on the rare-earth ion involved. The anisotropy of the exchange interaction acting on the rare-earth ion (represented by the tensor $\tilde{\lambda}$), which

TABLE II. Values of the additional bulk anisotropy constants at 4.2, 80, and 220 K calculated from the $Ho_xTb_{1-x}Fe_2$ spin-orientation diagram using the values $-0.04 a_0^{-1}$ for A_0/A_4, -150 K for $\mu_B H_{exch}(0)$, and 10 K$/a_0^4$ for A_4.

T (K)	4.2	80	220
K_1^{add} (10^6 erg/cm^2)	−9.7	−10.6	−0.92
K_2^{add} (10^6 erg/cm^2)	−160	−4.8	−2.7

TABLE III. Values of A_6/A_4 and A_4 based on point-charge model.

	Z—charge state of the iron ion			
	0	+1	+2	+3
A_4 (K/a_0^4)	27	16	5	−5.4
A_6/A_4 (a_0^{-2})	−0.008	−0.02	−0.05	0.06

has been neglected, is probably the main source of the remaining disagreements.

Transition Region

The theoretical model used in the present work predicts a first-order phase transition between the regions of different spin orientations. This prediction is in apparent contradiction with the presence of the transition regions in the spin-orientation diagrams. In the spectra corresponding to the transition of the direction of magnetization from the [110] to the [100] direction (Fig. 3 of the present work and Fig. 3 of Ref. 2) the two peaks at the extreme right have equal heights and the distance between them changes continuously: It is largest close to the [110] region and approaches zero close to the [100] region. Each spectrum in this transition region is a superposition of two six-line patterns of equal intensity. The difference between the fields, corresponding to the two patterns, changes continuously. It is largest close to the [110] direction and approaches zero close to the [100] region. These spectra cannot be interpreted as a superposition of two spectra, one corresponding to $\vec{n}$ being parallel to the [110] axis and the other to $\vec{n}$ being parallel to the [100] axis. They are consistent with the assumption that in this transition region $\vec{n}$ is in the (100) plane, but not parallel to any major crystal axis. Theoretically, such a behavior may be expected, since whenever the free energies calculated by the one-ion model are the same in the [110] and in the [100] directions, they will have the same value for $\vec{n}$ pointing in any direction in the (100) plane. In the region close to the theoretical boundary line in the spin-orientation diagram the free energies will depend only slightly on the direction of $\vec{n}$ in the (100) plane. The easy direction of magnetization in this region will therefore be determined by the additional, relatively weak, noncubic anisotropic interactions, and will change from the [110] to the [100] direction.

Each of the spectra corresponding to the transition regions between [111] and [110] or [111] and [100] directions of magnetization (Fig. 2 of Ref. 2 and Fig. 2) may be fitted in two ways: (i) as a superposition of two spectra, each of which corresponds to a different direction of magnetization parallel to one of the major axes; (ii) as corresponding to one direction of magnetization which is not parallel to any of the three major crystal axes.

The first fitting method assumes implicitly that the existence of the transition regions is a result of the inhomogeneity of the samples: Even though the samples were homogeneous with respect to the composition of the rare-earth ions, there may exist a statistical distribution of compositions of the two rare-earth species in the various elementary magnetic domains. Since this distribution has a certain width around the mean nominal composition, the spin reorientation may be smeared out over a range of compositions (and, therefore, of temperatures) corresponding to the width of the distribution of compositions.

It does not seem plausible that the inhomogeneity is the sole or main factor for the appearance of any of the transition regions, as a relatively large spread in the microscopic composition would also affect the spectra corresponding to the transition region between the [110] and [100] directions. As mentioned above, these spectra cannot be interpreted as a superposition of two spectra, one corresponding to $\vec{n} \parallel [110]$ and the other to $\vec{n} \parallel [100]$.

We tend to believe, therefore, that the appearance of the transition regions is due mainly to the existence of additional noncubic anisotropic terms, that have been neglected in Eq. (1) and have been discussed above. As a result of these terms, the magnetization may not coincide with the direction of one of the major crystalline axes and in the transition region may deviate significantly from these axes. Each of the different spectra obtained in the transition region corresponds to a different direction of $\vec{n}$ relative to the crystalline axes.

V. CONCLUSIONS

The present experimental data concerning the direction of magnetization of the $R_x^1 R_{1-x}^2 Fe_2$ compounds were described in terms of (x, T) spin-orientation diagrams. Theoretical spin-orientation diagrams were calculated assuming that the magnetocrystalline anisotropy is due to the anisotropy of the interaction between the $4f$ electrons of the rare-earth ions with the crystalline fields. These theoretical calculations reproduced the general features of the experimental results though small discrepancies remained. Adding to the calculated free energy of the crystals a contribution which originates mainly in the Fe-Fe interaction and is independent of the rare-earth ions involved improved the agreement between the theoretical and experimental spin-orientation diagrams. It seems that the remaining discrepancies between theory and experiment are a result of the neglect of noncubic anisotropic terms due to crystalline

distortion, dipolar fields, and especially the anisotropy of the Fe-R exchange interactions. These last terms are probably also responsible for the existence of the transition regions.

ACKNOWLEDGMENTS

We would like to thank B. Zarbiv and D. Dayan for help in preparing the samples and J. Mazor for carrying out the x-ray measurements.

[1]G. J. Bowden, D. St. P. Bunbury, A. P. Guimaraes, and R. E. Synder, J. Phys. C 2, 1367 (1968).
[2]U. Atzmony, M. P. Dariel, E. R. Bauminger, D. Lebenbaum, I. Nowik, and S. Ofer, Phys. Rev. Lett. **28**, 244 (1972).
[3]J. W. Colby, *Magic IV. A Computer Program for Quantitative Electron Microprobe Analysis* (Bell Telephone Laboratories, Allentown, Pa., 1969).
[4]M. T. Hutchings, in *Solid State Physics*, edited by H. Ehrenreich, F. Seitz, and D. Turnbull (Academic, New York, 1966), Vol 16, p. 277.
[5]A. J. Freeman and R. E. Watson, Phys. Rev. **127**, 2058 (1962).
[6]A. J. Freeman and R. E. Watson, Phys. Rev. 139, A1606 (1965).
[7]R. L. Cohen, Phys. Rev. 134, A94 (1964).
[8]E. Segal, Ph.D. thesis (Hebrew University, 1967) (unpublished).
[9]G. Will and M. D. Bargouth, Phys. Kondens. Mater. **13**, 137 (1971).
[10]Value of $\mu_B H_{\text{exch}}(0)$ was derived by S. Ofer, I. Nowik, and S. G. Cohen [in *Chemical Applications of Mössbauer Spectroscopy*, edited by V. I. Goldanskii and R. H. Herber (Academic, New York, 1968), p. 471] from results presented in Ref. 7.
[11]R. F. Pearson, J. Appl. Phys. **32**, 1236 (1962); Proc. Phys. Soc. Lond. **86**, 1055 (1965).
[12]G. K. Wertheim, V. Jaccarino, and J. W. Wernick, Phys. Rev. A **135**, 151 (1964).
[13]A. E. Clark and H. S. Belson, Phys. Rev. B **5**, 3642 (1972).
[14]H. G. Purwins, Z. Phys. **233**, 27 (1970).
[15]B. Bleaney, Proc. R. Soc. A **276**, 28 (1963).

PHYSICAL REVIEW B VOLUME 7, NUMBER 9 1 MAY 1973

Orbital Contributions to the Transferred Hyperfine Fields in Rare-Earth Compounds

B. D. Dunlap and I. Nowik
Argonne National Laboratory, Argonne, Illinois 60439*

Peter M. Levy†
Department of Physics, New York University, New York 10003

(Received 6 July 1972)

Magnetic hyperfine fields acting on the nuclei of diamagnetic atoms in rare-earth intermetallic compounds are generally assumed to follow a form $H_{\text{hf}}=H_s(g_J-1)\langle J_z\rangle$. However, such an expression is inadequate to describe the detailed dependence of the transferred hyperfine fields as the rare-earth ion is changed. It is shown that an expression based on a Hamiltonian which includes orbital contributions to the hyperfine field can describe the available data on several series of rare-earth compounds. This dependence has the form $H_{\text{hf}}=[(g_J-1)H_{01}+(2-g_J)H_{10}+c_nH_{21}]\langle J_z\rangle$, where the c_n are appropriate rare-earth reduced matrix elements. By fitting the extant data to this expression, we find that the orbital contributions H_{10} and H_{21} are appreciable. The general form of this expression is found to be valid for a variety of mechanisms which produce transferred and supertransferred hyperfine fields.

I. INTRODUCTION

The magnetic hyperfine field acting on the nuclei of diamagnetic atoms in rare-earth intermetallic compounds is generally considered to be a result of the s-f exchange interaction between conduction electrons and the rare-earth atoms. This produces a conduction-electron polarization which causes a hyperfine field on neighboring atoms directly through the contact interaction and indirectly through core polarization. Since both of these contributions are proportional to the conduction-electron polarization, measurements of the hyperfine fields have frequently been used in attempts to obtain information concerning the s-f interaction. In the most common approach, this interaction is written[1]

$$\mathcal{H}_{sf}=-2\Gamma_{sf}(g_J-1)\vec{J}\cdot\vec{s}_{\text{cond}}, \tag{1}$$

where Γ_{sf} is an exchange coupling parameter, g_J is the Landé g factor for a rare-earth ion with total angular momentum J, and $\vec{s}_{\text{cond}}$ is the conduction-electron spin. In a series of isostructural compounds in which the rare-earth atom is changed, the resulting conduction-electron polarization produces a hyperfine field H_{hf} at the nuclei of neighboring atoms which should vary with the rare-earth component according to